Title: Autism-associated Shank3 is essential for homeostatic plasticity and neuronal circuit stability

Authors: Vedakumar Tatavarty[1], Alejandro Torrado Pacheco[1], Heather Lin [1,†], Nathaniel J. Miska[1], Keith B. Hengen[1, §], Florence F. Wagner[2], Gina G. Turrigiano[1, *]

Affiliations:

[1] Dept of Biology, Brandeis University, Waltham, MA 02493.

[2] Stanley Center for Psychiatric Research, Broad Institute of Massachusetts Institute of Technology and Harvard University, Cambridge, MA.

† Current address: Emory University Medical School, Atlanta, GA,30322.

§ Current address: Dept of Biology, Washington University, St. Louis, MO 63130.

* To whom correspondence should be addressed: turrigiano@brandeis.edu.

Abstract

Mutations in Shank3 are strongly associated with autism spectrum disorders and circuit disfunction, but a unified view of how Shank3 loss disrupts circuit function and excitability is lacking. Stabilizing, homeostatic forms of synaptic and intrinsic plasticity are critical for preventing circuit hyper- or hypo-excitability, leading us to ask whether Shank3 loss perturbs circuits by disrupting homeostatic plasticity. We show that Shank3 loss abolishes synaptic and intrinsic homeostatic plasticity, which can be rescued by lithium, a drug with therapeutic potential in human Shankopathies. Further, Shank3 loss *in vivo*

severely compromises the ability of visual cortical circuits to recover from perturbations to sensory drive. Our findings suggest that the loss of homeostatic compensation is a critical endophenotype that can explain a range of circuit disfunctions in Shankopathies.

One Sentence Summary

Loss of the autism gene Shank3 impairs the resiliency of brain circuits by preventing homeostatic self-tuning

Main Text

Mutations in the multidomain scaffold protein Shank3 are associated with autism spectrum disorders (ASDs), Phelan-McDermid syndrome, and intellectual disability (*1*). Animal models of Shank3 loss have uncovered a number of circuit defects in a wide range of brain regions that might contribute to the behavioral phenotypes of these Shankopathies (*1-3*), but a unified view of how haploinsufficiency of Shank3 disrupts circuit function is lacking. A common feature of Shankopathies (as well as other monogenic ASDs) is the development of hyper- or hypoexcitability within specific CNS circuits (*4, 5*); because homeostatic plasticity normally serves to prevent such circuit imbalances from developing, this raises the intriguing possibility that defects in homeostatic plasticity represent a common endophenotype of monogenic ASDs (*5-7*). Here we ask whether this idea is relevant to Shankopathies, by determining the impact of Shank3 loss on the expression of homeostatic plasticity in rodent neocortical circuits both *in vitro* and *in vivo*.

In neocortex circuit stability is maintained through a set of homeostatic plasticity mechanisms, including synaptic scaling and intrinsic homeostatic plasticity, that cooperate to stabilize neuronal firing (*8-10*). Synaptic scaling bidirectionally scales all excitatory postsynaptic

strengths up or down in the right direction to compensate for prolonged perturbations in firing (*11*), while intrinsic homeostatic plasticity adjusts the input-output function of neurons by regulating the balance of inward and outward voltage-dependent conductances (*10, 12, 13*). In rodent primary visual cortex (V1) perturbing firing through monocular eyelid suture (MD) induces both types of homeostatic plasticity(*10, 14-16*), which cooperate to restore neuronal firing back to an individual firing rate set point(*8, 9*), a process referred to as firing rate homeostasis. While loss of Shank3 has been reported to modulate baseline synaptic transmission and intrinsic excitability in some brain regions and neuron types (*17-19*), a role for Shank3 in homeostatic plasticity has not been explored. Further, the possibility that defects in firing rate homeostasis (FRH) might contribute to circuit instability has not been tested in any ASD model.

Shank3 is a multidomain scaffold protein enriched at postsynaptic sites where it interacts with a number of synaptic scaling effector proteins (*4*). We found that synaptic scaling paradigms bidirectionally regulated the synaptic localization of Shank3: blocking spiking with tetrodotoxin (TTX) for 24 hr recruited both synaptic AMPA-type glutamate receptors (GluA2) and Shank3 to excitatory synapses (Fig 1A,B), while enhancing spiking with picrotoxin (PTX) for 24 hr reduced both GluA2 and Shank3 synaptic localization (Fig. 1B). To determine if a normal complement of Shank3 is necessary for synaptic scaling, we used RNAi to induce an acute and sparse knockdown (KD) of Shank3(*20*) to ~50% of control levels in individual pyramidal neurons (Fig. S1A,B). Shank3 KD (SH) had no significant impact on the basal amplitude of miniature excitatory postsynaptic currents (mEPSCs) compared to empty-vector (EV) controls (Fig. 1C-F), or on mEPSC frequency or excitatory synapse density (Fig. S2C,D). In contrast, Shank3 KD completely blocked both TTX-induced synaptic scaling up (Fig. 1C-F), and PTX-induced synaptic scaling down (Fig. 1G-H) of mEPSC amplitude, as well as the

changes in GluA2 synaptic accumulation that drive synaptic scaling (Fig. S2A, B, E and F). Synaptic scaling could be rescued by co-expression of an RNAi-resistant form of Shank3 (Fig. 1F, RES), ruling out off-target effects of the shRNA. Thus, a 50% loss of Shank3 (analogous to haploinsufficiency in human Shankopathies) is sufficient to completely abolish bidirectional synaptic scaling, and this requirement is cell-autonomous.

Lithium has wide efficacy to treat many neurological disorders, but the mechanism of action is debated (*21*). Several recent case studies suggest that lithium has therapeutic potential for treating human Shankopathies (*22-24*), leading us to wonder whether Li might rescue the synaptic scaling defect induced by Shank3 loss. After 24 hr incubation with a therapeutic dose (1 mM) of LiCl, Shank3 KD neurons were once again able to fully express synaptic scaling (Fig 2A,B). Li did not exert these effects through a simple global enhancement of synaptic scaling, as Li treatment had no impact on the magnitude of scaling in control neurons with a normal Shank3 complement (Fig. S3A,B). Further, although prolonged Li treatment (2 mM) is reported to reduce mEPSC amplitude in hippocampal neurons(*25*), here Li had no significant impact on basal postsynaptic (Fig. S4 B,C) or neuronal (Fig. S3) properties. GSK3 is a major target for lithium, that acts as a direct and indirect inhibitor of GSK3 through the inhibitory phosphorylation of Ser9/21 (*26*). We therefore tested a highly specific GSK3 inhibitor BRD0320 (GSK3i), that blocks GSK3 alpha and beta but not other closely related kinases (*27*), for its ability to rescue synaptic scaling. Like Li, BRD0320 was able to rescue synaptic scaling in Shank3 KD neurons (Fig. 2D), suggesting that the GSK3 pathway is dysregulated by Shank3 KD in neocortical pyramidal neurons, and contributes to the defect in synaptic scaling.

Shank3 interacts with ion channels as well as synaptic scaffold proteins (*18*), but the possibility that intrinsic homeostatic plasticity is impaired in shankopathies (or any other ASD

model) has not been explored. To determine whether Shank3 is essential for intrinsic homeostatic plasticity as well as synaptic scaling, we knocked down Shank3 as before, blocked spiking for 24 hr, and then probed intrinsic excitability by generating FI curves in the presence of synaptic blockers (Fig. 3). After TTX treatment the same current injection evoked more action potentials in EV neurons (Fig. 3A), and the entire FI curve shifted upward/leftward (Fig. 3B) as expected (*12*). Interestingly, although Shank3 KO reduces a hyperpolarization-activated cation current (I_h) and thus increases input resistant in hippocampal pyramidal neurons (*18*), Shank3 KD had no impact on passive neuronal properties (Fig. 3D,F) or on basal intrinsic excitability (Fig. 3B,C) in these neocortical pyramidal neurons; similarly, input resistance was not altered in L2/3 pyramidal neurons from Shank3 KO mice relative to WT littermates (Fig. 4.C,D., S5) . These data are consistent with the existence of cell type-specific differences in Shank3-ion channel interactions (*28*). Although baseline excitability was unaffected by Shank3 KD, intrinsic homeostatic plasticity was completely absent in Shank3 KD neurons (Fig 3B,C). Strikingly, we found that Li treatment could rescue intrinsic homeostatic plasticity (Fig. 3G,H) as well as synaptic scaling.

A major function of synaptic scaling and intrinsic homeostatic plasticity *in vivo* is to stabilize neuronal firing over long time scales through firing rate homeostasis(*8, 29*). Given that loss of Shank3 disrupts both of these major forms of homeostatic plasticity, we wondered whether firing rate homeostasis *in vivo* would also be disrupted. To test this, we implanted critical-period Shank3 KO(*17*) or littermate WT mice with multielectrode arrays in V1, performed MD, and followed changes in firing rates over time in freely behaving animals. In both WT and KO animals the distributions of baseline firing rates were wide as expected (*24, 30*), and were similar between WT and KO (Fig. 4A). MEPSC properties were also similar

between WT and KO L2/3 pyramidal neurons recorded in acute slices (Fig. 4C,D). In freely behaving WT mice MD resulted in biphasic changes in the firing of V1 neurons as expected (*8, 9*): first a drop in mean firing rates that reached a minimum after 3d of MD (due to suppressive Hebbian mechanisms induced by blurred vision through the closed eye (*31*)), followed by a homeostatic restoration of firing rates back to baseline values (Fig. 4E,F). However, the behavior of neurons in the KO was strikingly different: mean firing rates dropped as for WT animals, but there was no recovery in firing rates over the ensuing three days (Fig. 4E). In WT animals the entire distribution of firing rates initially shifted to the left, then recovered so by MD6 the distribution was indistinguishable from baseline (Fig 4F left). In contrast, in Shank3 KO mice the distribution shifted to the left and there was little recovery by MD6. These data indicate that loss of Shank3 severely compromises the ability of neocortical neurons to recover stable function after perturbations in drive; this normal recovery is either absent or dramatically slowed.

We have shown that normal Shank3 levels are essential for the expression of both synaptic scaling and intrinsic homeostatic plasticity. Because both forms of plasticity can be rescued by Li treatment, GSK3 hyperactivity is a likely common pathway by which Shank3 loss disrupts these two critical forms of homeostatic plasticity, and our data raise the possibility that rescue of homeostatic plasticity is an important mechanism of action of Li therapy. Synaptic scaling and intrinsic homeostatic plasticity play essential roles in experience-dependent plasticity within sensory systems(*32*), and although their roles in other brain regions remain largely unexplored, they are widely expressed (*33, 34*). Our data suggest that loss of synaptic scaling and intrinsic homeostatic plasticity severely impairs the ability of sensory circuits – and likely other circuits as well – to maintain stable firing in the face of sensory or other perturbations.

Many studies have documented alterations in circuit function in Shank3 KO mice, including disturbances in the distribution of firing rates (*30, 35*). Some circuits (striatum, neocortex) appear hyperexcitable (*30*), whereas other circuits (hippocampus, cingulate cortex and nucleus accumbens) appear hypoexcitable (*35, 36*), and a range of synaptic and excitability defects have also been reported across distinct brain regions, cell types, and developmental stages (*19, 28, 30, 37, 38*). Loss of MeCP2 (another monogenic ASD model) also impairs synaptic scaling and induces a similarly diverse set of changes to excitability in distinct brain regions (*5*). Our data suggest that some of this diversity in circuit and synaptic outcomes originates from fundamental defects in the homeostatic mechanisms that normally constrain excitability. When bidirectional homeostatic mechanisms are absent, neurons are at the mercy of perturbations to excitability driven by experience or development, and distinct perturbations to different circuits or cell types will drive a unique set of pathological changes in each brain region. Our findings suggest that the loss of key cellular mechanisms for homeostatic compensation is a critical endophenotype that can explain a range of circuit disfunctions in Shankopathies.

References and Notes:

1. C. Betancur, J. D. Buxbaum, SHANK3 haploinsufficiency: a "common" but underdiagnosed highly penetrant monogenic cause of autism spectrum disorders. *Mol Autism* **4**, 17 (2013).
2. Y. Zhou *et al.*, Mice with Shank3 Mutations Associated with ASD and Schizophrenia Display Both Shared and Distinct Defects. *Neuron* **89**, 147-162 (2016).
3. H. L. Wilson *et al.*, Molecular characterisation of the 22q13 deletion syndrome supports the role of haploinsufficiency of SHANK3/PROSAP2 in the major neurological symptoms. *J Med Genet* **40**, 575-584 (2003).
4. P. Monteiro, G. Feng, SHANK proteins: roles at the synapse and in autism spectrum disorder. *Nat Rev Neurosci* **18**, 147-157 (2017).
5. S. B. Nelson, V. Valakh, Excitatory/Inhibitory Balance and Circuit Homeostasis in Autism Spectrum Disorders. *Neuron* **87**, 684-698 (2015).
6. V. S. Dani *et al.*, Reduced cortical activity due to a shift in the balance between excitation and inhibition in a mouse model of Rett syndrome. *Proc Natl Acad Sci U S A* **102**, 12560-12565 (2005).
7. M. P. Blackman, B. Djukic, S. B. Nelson, G. G. Turrigiano, A critical and cell-autonomous role for MeCP2 in synaptic scaling up. *J Neurosci* **32**, 13529-13536 (2012).
8. K. B. Hengen, M. E. Lambo, S. D. Van Hooser, D. B. Katz, G. G. Turrigiano, Firing rate homeostasis in visual cortex of freely behaving rodents. *Neuron* **80**, 335-342 (2013).
9. K. B. Hengen, A. Torrado Pacheco, J. N. McGregor, S. D. Van Hooser, G. G. Turrigiano, Neuronal Firing Rate Homeostasis Is Inhibited by Sleep and Promoted by Wake. *Cell* **165**, 180-191 (2016).

10. M. E. Lambo, G. G. Turrigiano, Synaptic and intrinsic homeostatic mechanisms cooperate to increase L2/3 pyramidal neuron excitability during a late phase of critical period plasticity. *J Neurosci* **33**, 8810-8819 (2013).

11. G. G. Turrigiano, K. R. Leslie, N. S. Desai, L. C. Rutherford, S. B. Nelson, Activity-dependent scaling of quantal amplitude in neocortical neurons. *Nature* **391**, 892-896 (1998).

12. N. S. Desai, L. C. Rutherford, G. G. Turrigiano, Plasticity in the intrinsic excitability of cortical pyramidal neurons. *Nat Neurosci* **2**, 515-520 (1999).

13. A. Joseph, G. G. Turrigiano, All for One But Not One for All: Excitatory Synaptic Scaling and Intrinsic Excitability Are Coregulated by CaMKIV, Whereas Inhibitory Synaptic Scaling Is Under Independent Control. *J Neurosci* **37**, 6778-6785 (2017).

14. M. Kaneko, D. Stellwagen, R. C. Malenka, M. P. Stryker, Tumor necrosis factor-alpha mediates one component of competitive, experience-dependent plasticity in developing visual cortex. *Neuron* **58**, 673-680 (2008).

15. T. D. Mrsic-Flogel *et al.*, Homeostatic regulation of eye-specific responses in visual cortex during ocular dominance plasticity. *Neuron* **54**, 961-972 (2007).

16. T. Keck *et al.*, Synaptic scaling and homeostatic plasticity in the mouse visual cortex in vivo. *Neuron* **80**, 327-334 (2013).

17. J. Peca *et al.*, Shank3 mutant mice display autistic-like behaviours and striatal dysfunction. *Nature* **472**, 437-442 (2011).

18. F. Yi *et al.*, Autism-associated SHANK3 haploinsufficiency causes Ih channelopathy in human neurons. *Science* **352**, aaf2669 (2016).

19. Y. H. Jiang, M. D. Ehlers, Modeling autism by SHANK gene mutations in mice. *Neuron* **78**, 8-27 (2013).

20. C. Verpelli *et al.*, Importance of Shank3 protein in regulating metabotropic glutamate receptor 5 (mGluR5) expression and signaling at synapses. *J Biol Chem* **286**, 34839-34850 (2011).

21. C. Pisanu, C. Melis, A. Squassina, Lithium Pharmacogenetics: Where Do We Stand? *Drug Dev Res* **77**, 368-373 (2016).

22. J. I. M. Egger, W. M. A. Verhoeven, R. Groenendijk-Reijenga, S. G. Kant, Phelan-McDermid syndrome due to SHANK3 mutation in an intellectually disabled adult male: successful treatment with lithium. *BMJ Case Rep* **2017**, (2017).

23. S. Serret *et al.*, Lithium as a rescue therapy for regression and catatonia features in two SHANK3 patients with autism spectrum disorder: case reports. *BMC Psychiatry* **15**, 107 (2015).

24. H. Darville *et al.*, Human Pluripotent Stem Cell-derived Cortical Neurons for High Throughput Medication Screening in Autism: A Proof of Concept Study in SHANK3 Haploinsufficiency Syndrome. *EBioMedicine* **9**, 293-305 (2016).

25. E. S. Gideons, P. Y. Lin, M. Mahgoub, E. T. Kavalali, L. M. Monteggia, Chronic lithium treatment elicits its antimanic effects via BDNF-TrkB dependent synaptic downscaling. *Elife* **6**, (2017).

26. L. Freland, J. M. Beaulieu, Inhibition of GSK3 by lithium, from single molecules to signaling networks. *Front Mol Neurosci* **5**, 14 (2012).

27. F. F. Wagner *et al.*, Inhibitors of Glycogen Synthase Kinase 3 with Exquisite Kinome-Wide Selectivity and Their Functional Effects. *ACS Chem Biol* **11**, 1952-1963 (2016).

28. M. Zhu *et al.*, Shank3-deficient thalamocortical neurons show HCN channelopathy and alterations in intrinsic electrical properties. *J Physiol* **596**, 1259-1276 (2018).

29. G. G. Turrigiano, The dialectic of Hebb and homeostasis. *Philos Trans R Soc Lond B Biol Sci* **372**, (2017).

30. R. T. Peixoto, W. Wang, D. M. Croney, Y. Kozorovitskiy, B. L. Sabatini, Early hyperactivity and precocious maturation of corticostriatal circuits in Shank3B(-/-) mice. *Nat Neurosci* **19**, 716-724 (2016).

31. G. B. Smith, A. J. Heynen, M. F. Bear, Bidirectional synaptic mechanisms of ocular dominance plasticity in visual cortex. *Philos Trans R Soc Lond B Biol Sci* **364**, 357-367 (2009).

32. M. A. Gainey, D. E. Feldman, Multiple shared mechanisms for homeostatic plasticity in rodent somatosensory and visual cortex. *Philos Trans R Soc Lond B Biol Sci* **372**, (2017).

33. S. Glazewski, S. Greenhill, K. Fox, Time-course and mechanisms of homeostatic plasticity in layers 2/3 and 5 of the barrel cortex. *Philos Trans R Soc Lond B Biol Sci* **372**, (2017).

34. T. Keck *et al.*, Integrating Hebbian and homeostatic plasticity: the current state of the field and future research directions. *Philos Trans R Soc Lond B Biol Sci* **372**, (2017).

35. X. Wang *et al.*, Altered mGluR5-Homer scaffolds and corticostriatal connectivity in a Shank3 complete knockout model of autism. *Nat Commun* **7**, 11459 (2016).

36. O. Bozdagi *et al.*, Haploinsufficiency of the autism-associated Shank3 gene leads to deficits in synaptic function, social interaction, and social communication. *Mol Autism* **1**, 15 (2010).

37. W. Wang *et al.*, Striatopallidal dysfunction underlies repetitive behavior in Shank3-deficient model of autism. *J Clin Invest* **127**, 1978-1990 (2017).

38. M. Kouser *et al.*, Loss of predominant Shank3 isoforms results in hippocampus-dependent impairments in behavior and synaptic transmission. *J Neurosci* **33**, 18448-18468 (2013).

Acknowledgments: We thank Dr. Chiara Verpelli for Shank3 SH, Rescue and EV Constructs. We thank Lirong Wang, Genelle Rankin and Jorden Rabasco for technical support for culture experiments. We thank Ted Brookings for MATLAB program for analyzing *f*-I data.

Funding: This work was supported by Simons Foundation Award #: 345485 (GGT) and R37NS092635 (GGT).

Author contributions: Conceptualization: VT, GT; Methodology/software: VT, GT, ATP, KH, NM; Investigation: VT, NM, ATP, KH, HL; Formal Analysis, VT, ATP, NM, HL; Writing, VT, GT, ATP; Visualization, VT, ATP; Resources, FFW; Supervision/Administration/Funding, GT.

Competing interests: Authors declare no competing interests.

Data and materials availability: BRD0320was supplied by the Stanley Center for Psychiatric Research, and was confirmed to be of >95% purity based on HPLC LC-MS analysis (Alliance 2795, Waters). All data are presented in main text or supplementary materials, and will be made available upon request.

Supplementary Materials:

Materials and Methods

Figures S1-S5

Tables S1

Fig1

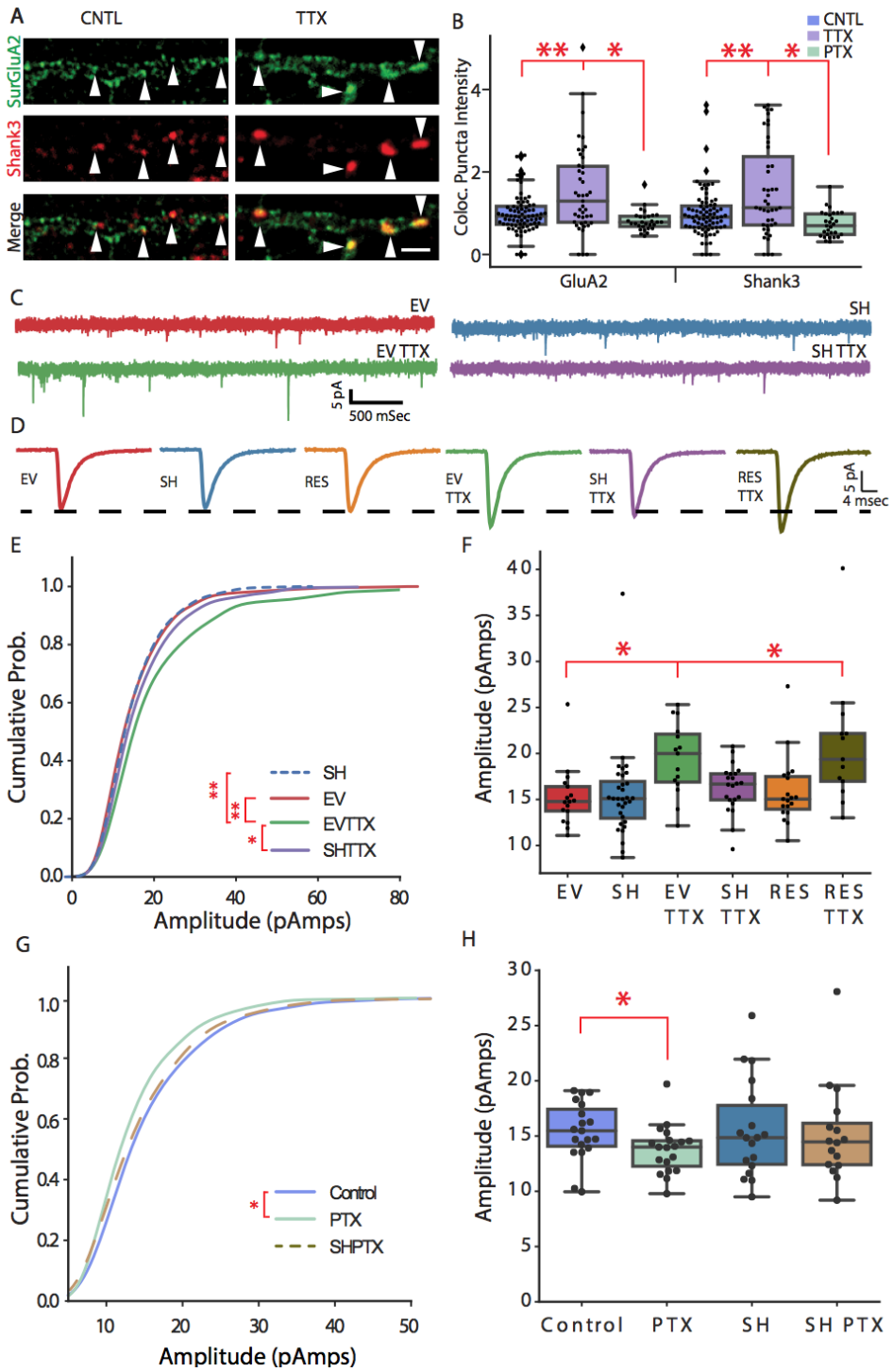

Figure 1. **Block of bidirectional synaptic scaling by Shank3 loss**. (**A**) Representative images of control (left) and TTX-treated (right) dendrites, immunolabled for surface GluA2 (green) and

Shank3 (red). Arrowheads indicate example colocalized puncta. Scale bar 2 µm. (**B**) Total intensity of GluA2 (left) and Shank3 (right) signal at colocalized sites after 24 hrs in TTX or PTX (*n*, Control = 80, TTX = 43, PTX = 29 neurons). ANOVA followed by Bonferroni correction (BC). (**C**) Example raw traces and (**D**) average mEPSCs waveforms for indicated conditions. (**E**) Cumulative histograms of mEPSC amplitudes. EV TTX vs EV (**); vs SH (**); vs SH TTX (*); Kruskal-Wallis (KW) test with BC (**F**) mean mEPSC amplitude, (*n*, EV = 17, EV TTX = 15, SH = 32, SH TTX = 22, RES = 19, RES TTX = 13), One-way ANOVA followed by BC. (**G**) Cumulative histograms of mEPSCs. Control vs PTX (**); vs SH PTX (N.S). KW test with BC. (**H**) Mean EPSC amplitude (*n*, Control = 19 PTX = 19, SH = 17, SH PTX = 18); two-tailed Student's t-test. SH PTX not different from SH, $p>0.05$. Here and below, **indicates $p<0.01$, * indicates $p<0.05$; $p>0.5$ considered N.S.

Fig 2.

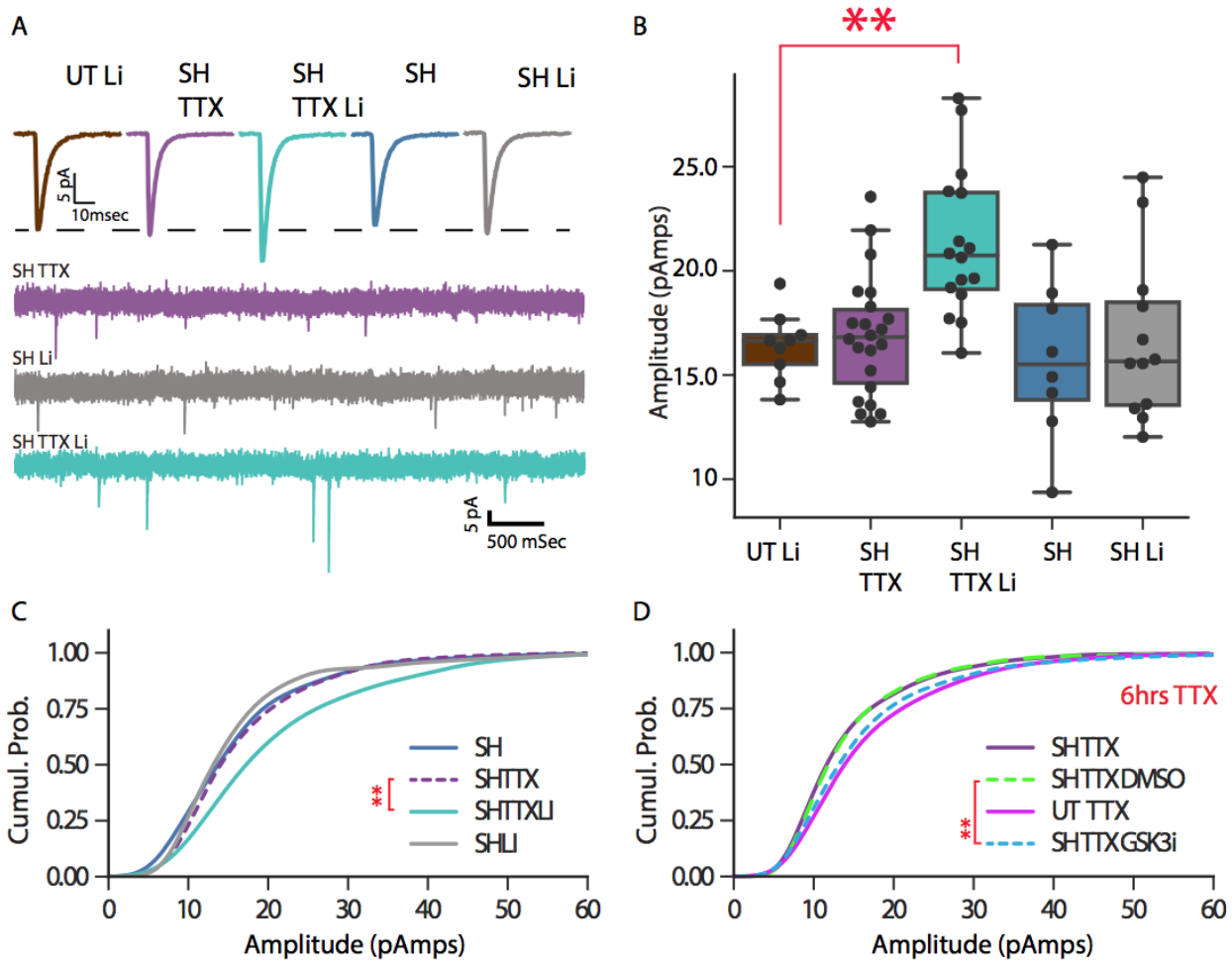

Fig. 2. LiCl treatment rescues synaptic scaling. (**A**) Average mEPSC traces (top) and example raw traces (below) from control or knockdown neurons treated with Li or Li + TTX for 24 hrs. (**B**) Mean mEPSC amplitudes (*n*, Li = 9 SH TTX = 22, SH TTX Li = 16, SH = 8, SH Li = 12). One-way ANOVA followed by BC. (**C**) Cumulative histograms of mEPSCs for conditions in (B) SH TTX Li vs SH TTX, SH Li, SH (**) KW test with BC. (**D**) Cumulative histograms from neurons treated for 6 hrs with TTX + DMSO (vehicle) or TTX + 5 µM GSK3 inhibitor (GSK3i) (*n*, UT TTX = 30, SH TTX = 25, SH TTX DMSO = 31, SH TTX GSK3i = 30. SH TTX GSK3i vs SH TTX DMSO (**), KW test, with BC.

Fig 3.

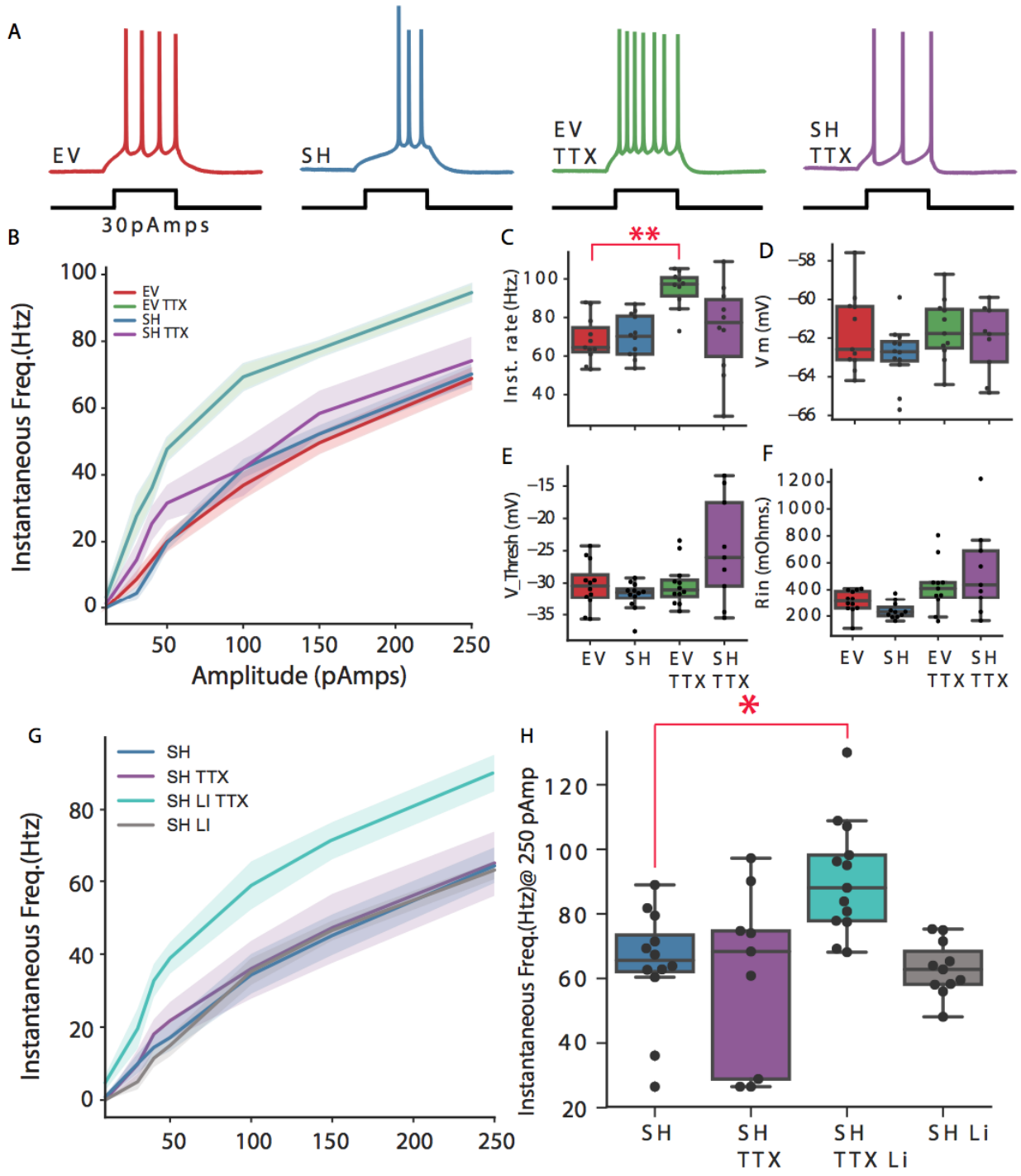

Figure 3. **Shank3 loss blocks, and Li rescues, intrinsic homeostatic plasticity.** (**A**) Example firing elicited with dc current injection from neurons in indicated conditions (**B**). Average *f*-I

curves for indicated conditions. Shaded area around curves denote S.E. (**C**). Average firing rates for indicated conditions during highest current injection (250 pA). (*n*, EV = 12, EV TTX = 12, SH = 11, SH TTX = 10). (**D-F**) Passive neuronal properties across conditions; VThresh = voltage threshold for action potential firing. (**G**) Li rescue: *f-I* curves for indicated conditions. (**H**). Average firing rates from conditions in (G) at highest current injection (250 pA). (*n*, SH = 13, SH TTX = 11, SH TTX Li = 13, SH Li = 11) One-way ANOVA with BC.

Fig 4.

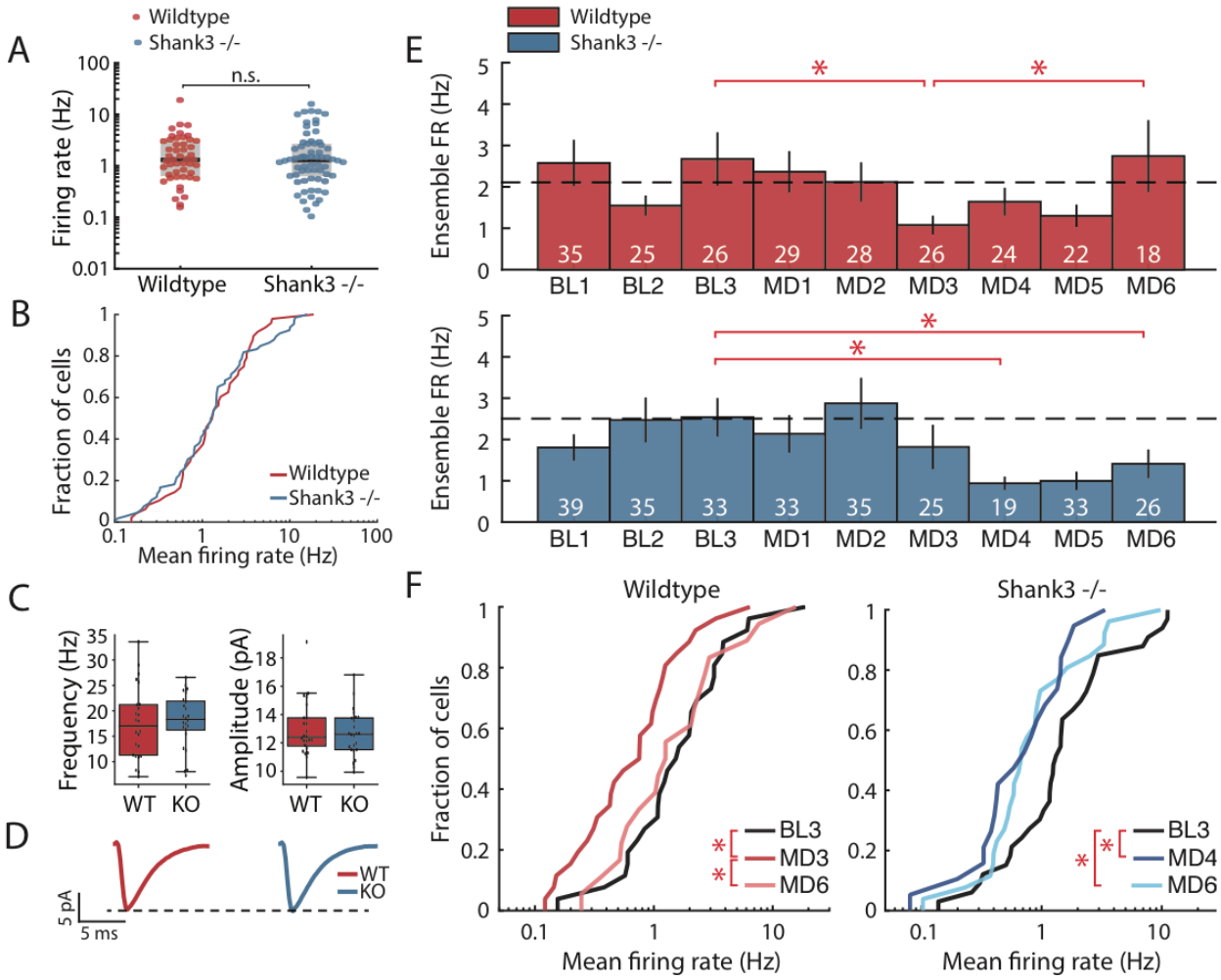

Shank3 is required for firing rate homeostasis *in vivo*. (A) Spontaneous mean firing rates in V1 of freely behaving mice at baseline (BL2 and BL3) for WT (left) and Shank3 KO (right) (N.S.), Wilcoxon rank-sum test. **(B)** Cumulative distributions of baseline firing rates. WT vs KO (N.S.), Anderson-Darling test. **(C)** Frequency (left) and amplitude (right) of V1 L2/3 pyramidal neuron mEPSCs (*n*, WT and KO = 24; two-sample t-test (N.S)). **(D)** Average mEPSC waveforms from WT or KO mice. **(E)** Ensemble average firing rates (Hz) in V1 of freely behaving mice during MD. KW test followed by pairwise Wilcoxon rank-sum tests with

Benjamini-Hochberg FDR procedure (BH-FDR). For WT: (BH-FDR): BL3 vs MD3, (*); MD3 vs MD6, (*); BL3 vs MD6, (N.S.). For KO: (BH-FDR): BL3 vs MD4, (*); MD4 vs MD6, (N.S.); BL3 vs MD6, (*). Bars show mean ± s.e.m. White numbers within bars indicate number of neurons. **(F)** Cumulative distributions of mean firing rates comparing baseline, early, and late MD. Anderson-Darling test followed by BH-FDR: for WT BL3 vs MD3, (*); MD3 vs MD6, (*); BL3 vs MD6, (N.S.). KO: BL3 vs MD4, (*); MD4 vs MD6, (N.S.); BL3 vs MD6, (*).